Mon. Not. R. Astron. Soc. **000**, 000–000 (0000) Printed 13 November 2015 (MN LATEX style file v2.2)

The cross-correlation analysis in Z source GX 349+2

G. Q. Ding[1⋆], W. Y. Zhang[1,2], Y. N. Wang[3], Z. B. Li[1], J. L. Qu[4] and C. P. Huang[1]

[1] *Xinjiang Astronomical Observatory, Chinese Academy of Sciences, 150, Science 1-Street, Urumqi, Xinjiang 830011, China*

[2] *University of Chinese Academy of Sciences, Beijing 100049, China*

[3] *Kapteyn Astronomical Institute, University of Groningen, PO BOX 800, NL-9700 AV Groningen, the Netherlands*

[4] *Key Laboratory for Particle Astrophysics, Institute of High Energy Physics, Chinese Academy of Sciences, Beijing 100049, China*

arXiv:1511.00599v2 [astro-ph.HE] 12 Nov 2015

ABSTRACT

Using all the observations from *Rossi X-ray Timing Explorer* for Z source GX 349+2, we systematically carry out cross-correlation analysis between its soft and hard X-ray light curves. During the observations from January 9 to January 29, 1998, GX 349+2 traced out the most extensive Z track on its hardness-intensity diagram, making a comprehensive study of cross-correlation on the track. The positive correlations and positively correlated time lags are detected throughout the Z track. Outside the Z track, anti-correlations and anti-correlated time lags are found, but the anti-correlated time lags are much longer than the positively correlated time lags, which might indicate different mechanisms for producing the two types of time lags. We argue that neither the short-term time lag models nor the truncated accretion disk model can account for the long-term time lags in neutron star low mass X-ray binaries (NS-LMXBs). We suggest that the extended accretion disk corona model could be an alternative model to explain the long-term time lags detected in NS-LMXBs.

Key words:
binaries: general — stars: individual (GX 349+2) — stars: neutron — X-rays: binaries

1 INTRODUCTION

X-ray binaries (XRBs), consisting of a compact object and a companion star, can be divided into low mass X−ray binaries (LMXBs) and high mass X−ray binaries (HMXBs) according to the mass of the companion star. The compact object is either a neutron star (NS) or a black hole (BH). Based on their spectral and timing properties, NS-LMXBs could be classified as Z sources and atoll sources (Hasinger & van der Klis 1989).

⋆ Email: dinggq@xao.ac.cn, dinggq@gmail.com.

The Z sources, with high luminosity close to the Eddington limit, trace out a Z-shape track on their hardness-intensity diagrams (HIDs), which are divided into three branches, called horizontal branch (HB), normal branch (NB), and flaring branch (FB), respectively. Among the six confirmed Z sources, Cyg X-2, GX 5-1, and GX 340+0 are called Cyg-like Z sources, and the other three Z sources, i.e. Sco X-1, GX 17+2, and GX 349+2, are referred to as Sco-like Z sources. On the HIDs of atoll sources with luminosity below $\sim 10^{38}$ ergs s^{-1}, two main segments are seen, which are called banana state (BS) and island state (IS), respectively; in the BS, the variation of hardness is relatively small, while their luminosity spans a wide range; however, in the IS, the variation of hardness is obvious, while the change of luminosity is relatively small and they are with the lowest luminosity (Church, Gibiec & Bałucińska-Church 2014). Furthermore, the segment of BS is split into two subsections, i.e. the lower banana (LB) with lower luminosities and the upper banana (UB) with higher luminosities. In general, atoll sources are either in IS or in BS depending on their luminosities. Generally, a Z source cannot become an atoll source and vice versa. However, two peculiar NS-LMXBs, i.e. Cir X-1 and XTE J1701-462, show Z source behaviors at relatively high luminosities, while they display atoll source behaviors at low luminosities (Oosterbroek et al. 1995; Shirey, Bradt & Levine 1999; Homan et al. 2007, 2010; Lin, Remillard & Homan 2009).

The spectral and timing analysis are two main methods for studying XRBs. Among the timing analyses, the cross−correlation analysis can be used to study the relation of light curves in two different energy bands. By analyzing the cross−correlation function (CCF) of light curves in two different energy bands, the correlation and time lag between soft and hard X−ray light curves can be obtained, which are useful and important to investigate the structures of accretion disk and the mechanisms for producing X-rays. According to the behaviors of CCFs, the correlations can be classified as anti−correlations, positive and ambiguous correlations, respectively. Anti−correlations correspond to negative cross−correlation coefficients (CCCs), while positive correlations correspond to positive CCCs. If no obvious correlations are presented in the CCFs, such correlations are called ambiguous correlations. Soft time lags mean that the lower energy photons reach behind, while hard time lags imply that the lower energy photons lead the higher energy photons. The cross−correlation analysis technique has been used to analyze the correlations of X-rays and long-term time lags from tens of seconds to over one thousand seconds in two energy bands of XRBs (e.g. Choudhury & Rao 2004; Lei et al. 2008, 2013; Wang, et al. 2014). In addition to the CCF method, the cross-spectral analysis is another important method for analyzing time lags (Nowak et al. 1999a), which has been widely used to investigate the short-term time lags in the order of milliseconds in XRBs (e.g. van der Klis et al. 1987; Miyamoto et al. 1988; Cui 1999; Qu, Yu & Li 2001; Qu et al. 2010a). In the past several decades, various time lags have been detected in XRBs through analyzing the

data from X-ray satellites, of which *RXTE* has contributed greatly (see review: Poutanen 2001).

GX 349+2, also known as Sco X-2, is a Sco-like Z source. Using the observations from *EXOSAT*, Ponman, Cooke & Stella (1988) detected quasi-periodic oscillations (QPOs) at ∼6 Hz in this source. Using observations from *Rossi X-ray Timing Explorer (RXTE)*, O'Neill et al. (2002) investigated the evolution of QPOs along a Z track on its HID and found QPOs at 3.3-5.8 Hz on the FB and at 11-54 Hz on the NB. Also through analyzing data from *RXTE*, Zhang, Strohmayer & Swank (1998) detected a twin kilohertz (kHz) QPOs with lower and upper frequencies of 712 Hz and 978 Hz, respectively. In particular, the kHz QPOs were only found at the top of the NB. Using the *RXTE* data for this source, Agrawal & Sreekumar (2003) carried out the spectral evolution on its Z track. They fitted the spectra in 2.5-25 keV using a two-component model consisting of a disk blackbody and a Comptonized component representing Comptonization in the central hot corona or the boundary layer, which could act as the Eastern model (Mitsuda et al. 1984, 1989). However, Church et al. (2012) used another two-component model consisting of a blackbody and a cut-off power law representing Comptonization in an extended corona above the disk to fit the spectra of the Sco-like Z sources, including GX 349+2. Using the data from *BeppoSAX*, Di Salvo et al. (2001) studied its broadband spectra (0.1−200 keV) and a hard tail was detected in this source. Moreover, they detected an absorption edge at ∼9 keV in the spectra. Using the observation from XMM, Iaria et al. (2009) performed spectral analysis of GX 349+2. They fitted the continuum in the 0.7-10 keV energy range with the Eastern model (Mitsuda et al. 1984). Significantly, Iaria et al. (2009) found several broad emission features below 4 keV and a broader emission feature in the Fe-K_α region in the spectra and proposed that these relativistic lines are formed due to the reflection in the inner disk region that is illuminated by the emission around the NS. The relativistic Fe-K emission line of GX 349+2 was also detected in its *Suzaku* spectra (Cackett et al. 2008).

In this work, using all the data from the proportional counter array (PCA) on board *RXTE* for GX 349+2, we systematically investigate the cross-correlation correlations between soft and hard light curves of this source. We describe our data analyses in section 2, present our results in section 3, discuss our results in section 4, and, finally, give our conclusions in section 5.

2 DATA ANALYSIS

RXTE made 138 observations from 1996 to 2011 for Z source GX 349+2, including 23 observations from January 9 to January 29, 1998, during which the source evolved on the most extensive NB+FB tracks ever reported on its HID (O'Neill et al. 2002).

With HEASOFT 6.11 and all the *RXTE* observations for GX 349+2, we systematically perform cross-correlation analysis for this source. In our analysis, only PCA data are needed. The PCA consists of five identical proportional counter units (PCUs) in energy range 2−60 keV (Jahoda et al. 2006). We use the data during the intervals when all five PCUs were working. The PCA Standard 2 mode data with bin size of 16 s are used to produce light curves with *RXTE* FTOOLS SAEXTRCT. Then, with RUNPCABACKEST, a *RXTE* script, we produce the background files from the bright background model (pca_bkgd_cmbrightvle_eMv20051128.mdl) provided by *RXTE* team and thus produce the background light curves. Finally, applying LCMATH, a XRONOS tool, we generate the background-subtracted light curves with various energy bands. When extracting light curves, good time intervals (GTIs) are restricted through inputting GTI files, which are created with the FTOOLS MAKETIME obeying criteria: the earth elevation angle greater than 10° and the pointing offset less than 0.02°.

To build the HID on which the source traced out the most extensive Z track, following O'Neill et al. (2002), we define the hardness as the count rate ratio between 8.7−19.7 keV and 6.2−8.7 keV energy bands, and the intensity as the count rate in the 2.0−19.7 keV energy band. The produced HID is shown by Figure 1. In order to investigate the evolution of cross-correlation correlations along the Z track, we divide the track into 23 regions. For minimizing the variation of count rate and meanwhile having enough observation time in each region, these regions are produced obeying the criteria: the count rate variation in each region is less than 1500 count s^{-1} except the region No. 23; the hardness variation in each of the regions in the NB and in the first half FB is less than 0.025, while it is less than 0.5 for each region in the second half FB, because, here, the points are scattered. Then, we study the evolution of cross-correlation correlations between hard and soft X-ray light curves along the Z track. Firstly, based on the values of hardness and count rate in each region, we determine the relative and absolute time intervals of each region with FTOOLS MAKETIME and TIMETRANS, respectively. Secondly, inputting the absolute time intervals of each region when light curves are extracted, we produce the soft and hard X-ray background-subtracted light curves of each region in 2-5 keV and 16-30 kev energy bands, respectively. Thirdly, with XRONOS TOOL CROSSCOR, we generate the CCF between the soft and hard background-subtracted light curves of each region. To get the CCCs and time lags, we fit the CCFs with an inverted Gaussian function at a 90% confidence level. The results of the 23 regions are listed in Table 1. The total relative time length of each of the 23 regions spans from 1072 s to 8606 s and the absolute time intervals of each region spread within 2 days.

As shown in Figure 1, the track consists of an extensive NB and an elongated FB, respectively. Regions 1-10 constitute the NB, while regions 11-23 make up the FB. In order to describe the positions of the 23 regions on the NB+FB tracks, the segment of

regions 1-3 is called upper NB (UNB), the segment of regions 4-6 is called middle NB (MNB), and the segment of regions 7-10 is called lower FB (LFB); similarly, the segment of regions 11-15 is named lower FB (LFB), the segment of regions 16-18 is named middle FB (MFB), and the segment of regions 19-23 is named upper FB (UFB). The intensity as a function of time during the HID is shown in Figure 2, in which the positions of various time intervals on the HID are marked. As shown in Figure 2, the two panels of the first row dominate the FB positions, while the two panels of the second row and the left panel of the third row are occupied by the NB positions, showing that the source evolves from the FB to the NB on the NB+FB tracks; the right panel of the third row and the left panel of the fourth row show the next evolutionary cycle from the FB to the NB; the right panel of the fourth row shows the beginning of the third evolutionary cycle. Therefore, the source regularly evolved on the HID during each evolutionary cycle, which leads to that the data of each region spread within two days. For Fourier analysis, unbroken sections of data are needed. Certainly, for cross-correlation analysis continuous observations should be better than broken observations. Here, although the observations within the HID span 21 days, yet the data within each region do not spread across very different observations, which ensures the validity of our results.

In addition, we perform cross-correlation analysis between soft and hard X-ray light curves for all the observations outside the period during which the source traced out the most extensive NB+FB tracks on its HID. Similarly, we produce the soft and hard X-ray background-subtracted light curves of each observation and then get its CCF, CCC, and time lag. It is noted that if there are several segments in the light curves of an observation, we produce the CCF of each segment.

3 RESULTS

In this work, using all the 138 *RXTE* observations from 1996 to 2011 for Z source GX 349+2, we systematically perform cross-correlation analysis between 2-5 kev and 16-30 keV light curves with the CCF method. The source traced out the most extensive Z track on the HID during the 23 observations from January 1 to January 29, 1998. Among the 23 regions on the HID, positive correlations and ambiguous correlations are detected in 18 and 5 regions, respectively, while anti-correlations are not found throughout the Z track. The HID positions of the 18 regions, the derived CCCs and time lags, and hardness values are listed in Table 1. Figure 3 and Figure 4 show two detected positive correlations and one ambiguous correlation, respectively. Eight regions of the 18 regions with detected positive correlations are assigned to the NB and other ten regions are belonged to the FB. Among the five regions with ambiguous correlations, the NB and FB host two and three regions, respectively. Fortunately, among the observations outside the period during

which the source traced out the most extensive Z track on its HID, the anti-correlations are detected in ten observations. The analysis results of these anti-correlations are listed in Table 2 and two representative anti-correlations are shown in Figure 5. The derived anti-correlated time lags vary between tens of seconds and thousands of seconds. Among the ten observations with anti-correlations, hard and soft X-ray time lags are detected in four and six observations, respectively. In one hundred observations outside the HID period, positive correlations are detected, which are listed in Table 3, while ambiguous correlations are found in five observations outside the HID episode. The anti-correlations, positive correlations, and ambiguous correlations are detected in 8.7%, 87%, and 4.3% of the total observations outside the HID period, respectively. Comparing the time lags listed in Tables 1-3, one can see that the positively correlated time lags vary from several seconds to tens of seconds, whereas the anti-correlated time lags span a wide range from tens of seconds to thousands of seconds, so the anti-correlated time lags of GX 349+2 are much larger than its positively correlated time lags, which is consistent with what was found in atoll source 4U 1735-44 and 4U 1608-52, as well as peculiar source XTE J1701-462 (Lei et al. 2013, 2014; Wang et al. 2014). It should be informed that a small number of short-term time lags less than one second are obtained in the positive correlations of GX 349+2, as listed in Tables 1 and 3.

4 DISCUSSION

4.1 The short-term time lags in XRBs

Through cross-spectral analysis, the short-term time lags (<1 s) between the emissions of two adjacent X-ray energy bands have been detected in a few Galactic black hole X-ray binaries (BHXBs) and NS-LMXBs. Among the BHXBs in which short-term time lags were studied, the short-term time lag behaviors of Cyg X-1 were investigated most deeply (Miyamoto et al. 1988, 1992; Crary et al. 1998; Nowak et al. 1999a; Pottschmidt et al. 2000; Negoro, Kitamoto & Mineshige 2001). The short-term time lags were also detected in microquasar GRS 1915+105 (Cui 1999; Reig 2000; Pahari et al. 2013), in GX 339-4 (Miyamoto et al. 1992; Nowak, Wilms & Dove 1999b), as well as in black hole candidate GS 2013+338 and GRO J0422+32 (Miyamoto et al. 1992; van der Hooft et al. 1999). The short-term time lags with values of several milliseconds were also found in NS-LMXBs, such as in Cyg X-2 and GX 5-1 (van der Klis et al. 1987; Vaughan et al. 1994) as well as in Cir X-1 (Qu, Yu & Li 2001; Qu et al. 2010b). Generally, the hard X-ray short-term time lags were detected in the hard states of BHXBs, while both hard and soft X-ray short-term time lags were detected in NS-LMXBs (van der Klis et al. 1987; Qu, Yu & Li 2001).

Some models have been proposed to explain short-term time lags, but the observed

various short-term time lags cannot be explained by any single model. The cross-spectral analysis technique is based on the Fourier transform, so the time lag spectrum, i.e. the correlation between the short-term time lag and the frequency of Fourier transform can be obtained. Usually, the short-term time lag is anti-correlated with Fourier frequency (van der Klis et al. 1987; van der Hooft et al. 1999; Nowak et al. 1999a; Nowak, Wilms & Dove 1999b; Pottschmidt et al. 2000; Qu et al. 2010a). Among the Fourier frequencies, some are the frequencies of QPOs, sequentially leading to that the short-term time lag is also anti-correlated with QPO frequency. Since the short-term time lag is in connection with the QPO parameter, it could be feasible to invoke the models responsible for QPOs to account for the short-term time lags, such as the shot model (Terrell 1972). In the shot model, it is assumed that the gravitation energy of accreting matter is transformed to thermal energy emitted as successive bursts, which are called "shots" and responsible for QPOs; the different shot profiles or shot distribution in different energy bands results in the time delays between the hard and soft X-ray emissions (Miyamoto & Kitamoto 1989; Nowak 19994; Nowak, Wilms & Dove 1999b; Poutanen 2001). Although the shot model provided an explanation for the strong aperiodic variability of the flux of accreting XRBs immediately after such variability was discovered and it was very early applied to account for the short-term lags, yet this model inevitably encountered difficulty when it was used to explain the large X-ray variability timescale range (Uttley & McHardy 2001; Churazov, Gilfanov & Revnivtsev 2001; Revnivtsev et al. 2009) and the linear rms-flux relation (Uttley & McHardy 2001; Ingram & van der Klis 2013). Since the shot model, various models have been proposed to explain the QPOs in XRBs, such as the beat-frequency models (Strohmayer et al. 1996; Ford et al. 1997; Miller, Lamb & Psaltis 1998), which were refuted by the fact that the observed QPO peak separation is not a constant (van der Klis 2000), the Lense-Thirring precession model (Stella & Vietri 1998), and the propagating fluctuation model (Ingram & Done 2011), etc. Using their propagating fluctuation model, Ingram & van der Klis (2013) explained the anti-correlation between the short-term time lag and the Fourier frequency well. There may be a prospect of interpreting the short-term time lags observed in XRBs with the help of these QPO models, whereas it is out of the scope of this paper.

Certainly, Comptonization is a common physical process for producing X-rays in XRBs, so it is widely invoked to interpret the observed time lags in the order of milliseconds in these sources (van der Klis et al. 1987; Ford et al. 1999; Nobili et al. 2000; Lee, Misra & Taam 2001; Poutanen 2001). In the Comptonization model, the low-energy seed photons, emitted from a relatively cool region such as the accretion disk, are inversely Comptonized by the energetic electrons from a hot source such as a hot corona or the hot plasma near the compact objects, in which the low-energy photons gain energy, while the high-energy electrons lose part of their energy, leading to that high-energy photons

undergo more inverse Compton scatterings and, therefore, they escape later than the low-energy photons, resulting in hard X-ray time lags (Ford et al. 1999). Obviously, soft X-ray time lags cannot be explained by this model. van der Klis et al. (1987) proposed that the softening of shots could account for soft time lags. In order to explain the time lags of GRS 1915+105, Nobili et al. (2000) proposed a scenario in which a standard thin disk (Shakura & Sunyaev 1973) coexists with a central corona with two parts, an inner part with relatively high temperature and an outer part with relatively low temperature. In the inner part, the inverse Compton scattering is taken place, resulting in hard X-ray time lags. However, in the outer part, the disk seed photons are Comptonized by the relatively cool electrons, in which the electrons gain energy, while the seed photons lose energy, so the low-energy photons undergo more Compton scatterings and escape later than high-energy photons, leading to soft X-ray time lags. Qu, Yu & Li (2001) invoked this scenario to explain the detected soft and hard X-ray time lags less than ten milliseconds in Cir X-1. In addition to the two models, there are some other models for explaining the short-term time lags of XRBs, such as the magnetic flare model (Poutanen & Fabian 1999). In this model, it is assumed that the X-rays are produced in compact magnetic flares and the movement for magnetic loops to inflate and detach from the accretion disk induces spectral evolution, which results in time lags corresponding to the evolution timescales of the flares.

4.2 The long-term time lags in XRBs

Through CCF technique, the long-term time lags ranging from hundreds of seconds to over one thousand seconds between hard and soft X-rays have been detected in a few Galactic BH X-ray binaries (BHXBs). Anti-correlated long-term hard X-ray time lags were first detected in the low/hard state of the high-mass BHXB Cyg X-3 (Choudhury & Rao 2004), then this kind of hard X-ray time lags were found in microquasar GRS 1915+105 during its χ states (Choudhury et al. 2005). It is noted that the χ states of this microquasar are the closest analog to the low/hard states of BHXBs. In addition, the similar long-term anti-correlated hard X-ray time lags were also detected in another microquasar XTE J1550-564, but in its very high state or steep power law state (Sriram et al. 2007). Interestingly, the long-term soft X-ray time lags of microquasar GX 339-4 were found in its hard and soft intermediate states (Sriram, Rao & Choi 2010). It is noted that the spectral pivoting was shown during the episodes when this kind of time lags were detected in these BHXBs (Choudhury & Rao 2004; Choudhury et al. 2005; Sriram et al. 2007). Choudhury & Rao (2004) proposed a truncated accretion disk model to explain the detected anti-correlated long-term hard X-ray time lags in BHXBs. In the scenario of this model, the optically thick accretion disk, where the soft X-rays are emitted, is truncated far away from the BH, while the truncated area, i.e. the high-temperature region between the inner disk

edge and the location near the BH, is full of Compton cloud which is responsible for the hard X-ray emission. Any change in the disk will trigger corresponding anti-correlated change in the Compton cloud in a viscous timescale, during which the accreting matter flows from the optically thick accretion disk to the truncated area, resulting in that the hard X-rays emitted in the Compton cloud lag behind the soft X-rays emitted in the disk.

Through the CCF method, the anti-correlated long-term hard time lags from tens of seconds to hundreds of seconds were also detected in a few NS-LMXBs. Lei et al. (2008) first detected anti-correlated long-term hard X-ray time lags in Z source Cyg X-2 and, meanwhile, anti-correlated long-term soft X-ray time lags were also found in this source. Sriram, Choi & Rao (2012) reported the similar anti-correlated long-term hard and soft X-ray time lags detected in another Z source GX 5-1. Moreover, in atoll source 4U 1735-44 and 4U 1608-52, Lei et al. (2013, 2014) detected four types of long-term X-ray time lags, i.e. anti-correlated long-term hard and soft X-ray time lags and positively correlated long-term hard and soft X-ray time lags. Wang et al. (2014) systematically investigated the cross-correlation evolution of XTE J1701-462 on its HIDs, detected the four types of long-term X-ray time lags, and found that its cross-correlation behavior evolves with luminosity. The model of truncated accretion disk was invoked to explain the detected long-term time lags in NS-LMXBs (Lei et al. 2008; Sriram, Choi & Rao 2012; Wang et al. 2014). However, we argue that the model of truncated accretion disk cannot account for the detected long-term time lags in NS-LMXBs. Firstly, this model can only account for the anti-correlated long-term hard X-ray time lags, while anti-correlated long-term soft X-ray time lags are usually detected in NS-LMXBs. Secondly, the truncated accretion disk model requires that an optically thick accretion disk is far away from the compact object, while the accretion disk of NS-LMXBs touches the NS (Inogamov & Sunyaev 1999, 2010). Here, we argue that in NS-LMXBs, the accretion disk touches the NS because of the absence of a magnetoshpere around the NS in these systems. In the XRBs hosting a strongly magnetized NS with surface magnetic field strength $B_0 \sim 10^{12}$ G, e.g. accretion-powered X-ray binary pulsars, most of which are NS-HMXBs, a magnetosphere will be formed around the NS (Lamb, Pethick & Pines 1973). In these XRBs, when the accreting matters approach the magnetosphere, they will be channeled onto the polar caps of the NS along the magnetic field lines, producing X-ray pulsations, which could be an evidence for a magnetosphere in XRBs. Additionally, cyclotron lines are usually observed in the X-ray spectra of accretion X-ray pulsars (Coburn et al. 2002; Caballero & Wilms 2012), showing sufficient B_0 to form a magnetosphere. Sequentially, in NS-HMXBs, the magnetic pressure from the magnetosphere pushes the accretion disk outwards, leading to that the disk might be far away from the NS. However, B_0 of NS-LMXBs, including Z sources and atoll sources, spans a range of $\sim 10^7 - 10^9$ G (Focke 1996; Campana 2000; Ding et al. 2006, 2011), which is much smaller than that of strongly magnetized NSs, so that it is

unlikely for a magnetosphere to be formed in NS-LMXBs. Actually, the X-ray pulsations have never been observed in Z sources and atoll sources except Aql X-1 (Casella et al. 2008) and cyclotron lines have never been observed in these sources too, any of which conforms the absence of a magnetosphere in NS-LMXBs. In the case of the absence of a magnetosphere, the accretion disk will reach the NS. Therefore, the accretion disk of NS-LMXBs touches the NS.

4.3 The long-term time lags in GX 349+2

In this work, using all the 138 *RXTE* observations from 1996 to 2011 for Z source GX 349+2, we systematically perform cross-correlation analysis between 2-5 kev and 16-30 keV light curves with CCF method. The results are listed in Tables 1-3 and selectively shown by Figures 3-5.

As reviewed and pointed out above, the long-term hard X-ray time lags of BHXBs can be explained by the truncated accretion disk model (Choudhury & Rao 2004; Choudhury et al. 2005; Sriram et al. 2007), but this model cannot account for the long-term time lags of NS-LMXBs, because the accretion disk in NS-LMXBs actually contacts with the NS (Church & Bałucińska-Church 2004; Inogamov & Sunyaev 1999, 2010). Moreover, the long-term time lags detected in XRBs, including the results that we obtain in this work, are larger than dozens of seconds, even over one thousand seconds, while the short-term time lags in XRBs spans in the range of milliseconds, so it is a feasible assumption that the mechanisms responsible for the long-term X-ray time lags could be very different from those models accounting for the short-term time lags in XRBs, such as the shot model reviewed above. Besides, in general, the short-term time lags are derived from two light curves in two adjacent energy bands, e.g. 2-5 keV vs. 5-13 keV for GRS 1915+105 (Reig 2000) and 1.8-5.1 keV vs. 5.1-13.1 keV for Cir X-1 (Qu, Yu & Li 2001), while the long-term time lags are usually derived from two light curves with distant energy bands, e.g. 2-7 keV vs. 20-50 keV for Cyg X-3 (Choudhury & Rao 2004) and 2-5 keV vs. 16-30 keV for GX 5-1 (Sriram, Choi & Rao 2012), which indicates that the X-rays responsible for the short-term time lags come from two adjacent emission regions, even from the same area, while the the X-rays producing long-term time lags might come from two regions which are far away each other.

Here, we invoke an extend accretion disk corona (ADC) model to explain the long-term time lags detected in NS-LMXBs, including the long-term time lags of GX 349+2 that we derive in this work. Analyzing the dip and non-dip spectra of NS-LMXBs, Church & Bałucińska-Church (1993, 1995) proposed a Birmingham model which consists of a blackbody component interpreted as the emission from a point source, i.e. the NS, and a power law component that might be resulted from the Comptonization of thermal emission in an ADC above the accretion disk. Through dip ingress time tech-

nique, Church & Bałucińska-Church (2004) measured the radius of the ADC and developed the Birmingham model into an extended ADC model. The measured radius of a thin, hot corona above the accretion disk varies in the range of $\sim$(2–70)$\times10^4$ km. Therefore, the corona is very extended and the disk is substantially covered by the corona. In the extended ADC model, almost all soft X-ray photons from the accretion disk are inversely Comptonized by the energetic electrons from the extended ADC, which produces the observed hard X-rays, while the observed soft X-rays are interpreted as the emission from the NS; the accretion disk is illuminated by the emission of the NS, leading to the production of the extended ADC above the disk. This model was successfully applied to Cyg-like Z sources (Church, Halai & Bałucińska-Church 2006; Jackson, Church & Bałucińska-Church 2009; Bałucińska-Church et al. 2010) and Sco-like Z sources (including GX 349+2) (Church et al. 2012), as well as atoll sources (Church, Gibiec & Bałucińska-Church 2014), so it could be a universal model for NS-LMXBs. Since the extended ADC model is a unified model for NS-LMXBs, we try to interpret the long-term time lags in NS-LMXBs with the help of this model. The extended ADC and the NS are two independent emitting regions, which satisfies the request that the hard and soft X-rays for long-term time lags are emitted from two distant regions, as discussed above. In order to explain the long-term time lags detected in NS-LMXBs in terms of the extended ADC model, we introduce two timescales. One is the Comptonization timescale during which the disk seed photons are inversely Comptonized by the high-energy electrons in the extended ADC, and another is the viscous timescale in the order of hundreds of seconds (Lei et al. 2008), during which the accreting matter flows from the disk onto the NS. The hard X-ray time lags will be produced if the Comptonization timescale is less than the viscous timescale, and, contrarily, the soft X-ray time lags will be observed if the Comptonization timescale is larger than the viscous timescale. It is noted that a minority of positively correlated short-term time lags ($<$1 s) are listed in Tables 1 and 3, which are derived with the CCF method in our work. These short-term time lags cannot be explained by the models reviewed in section 4.1, because those models are used to interpret the short-term time lags produced in two adjacent energy intervals, while these short-term time lags obtained in this work are derived from two distant energy intervals, i.e. 2-5 kev and 16-30 keV energy intervals. In the frame of the extended ADC model, we propose that these short-term time lags will be observed under the circumstance that the Comptonization timescale is comparable with the viscous timescale.

5 CONCLUSION

In this work, using all the *RXTE* observations for Z source GX 349+2, we systematically perform cross-correlation analysis between soft and hard X-rays with CCF method. Positive correlations and corresponding hard and soft X-ray long-term time lags are detected throughout an extensive Z track on its HID. Anti-correlated correlations and anti-correlated soft and hard X-ray long-term time lags are found outside the HID. It is noted that in most observations outside the HID, positive correlations and positively correlated hard and soft long-term X-ray time lags are also obtained. We review the short-term time lags obtained with the Fourier cross-spectral analysis in XRBs and some models responsible for the short-term time lags. We also review the long-term hard X-ray time lags found in BHXBs, which can be explained by the truncated accretion disk model. We argue that the long-term X-ray time lags in NS-LMXBs cannot be interpreted by those models responsible for the short-term time lags or the truncated accretion disk model. We invoke the extended ADC model to explain the long-term X-ray time lags in NS-LMXBs, including GX 349+2.

ACKNOWLEDGEMENTS

We thank the anonymous referee for her or his constructive comments and suggestions, which helped us carry out this research and improve the presentation of this paper. This research has made use of the data obtained through the High Energy Astrophysics Science Archive Research Center (HEASARC) On-line Service, provided by NASA/Goddard Space Flight Center (GSFC). This work is partially supported by the 2014 Project of Xinjiang Uygur Autonomous Region of China for Flexibly Fetching in Upscale Talents, National Key Basic Research Program of China (973 Program 2015CB857100), the Natural Science Foundation of China under grant nos. 11173024 and 11203064, and the Program of the Light in Chinese Western Region (LCWR) under grant no. XBBS 201121 provided by Chinese Academy of Sciences (CAS).

REFERENCES

Agrawal V. K., Sreekumar P., 2003, MNRAS, 346, 933

Bałucińska-Church M., Gibiec A., Jackson N. K., Church M. J., 2010, A&A, 512, A9

Caballero I., Wilms J., 2012, Mem. Soc. Astron. Ital., 83, 230

Cackett E. M., Miller J. M., Bhattacharyya S., Grindlay J. E., Homan J.; van der Klis M., Miller M. C., Strohmayer T. E., Wijnands R., 2008, ApJ, 674, 415

Campana S., 2000, ApJ, 534, L79

Casella P., Altamirano D., Patruno A., Wijnands R., van der Klis M., 2008, ApJ, 674, L41

Choudhury M., Rao A. R., 2004, ApJ, 616, L143

Choudhury M., Rao A. R., Dasgupta S., Pendharkar J., Sriram K., Agrawal V. K., 2005, ApJ, 631, 1072

Churazov E., Gilfanov M., Revnivtsev M., 2001, MNRAS, 321, 759

Church M. J., Bałucińska-Church M., 1993, MNRAS, 260, 59

Church M. J., Bałucińska-Church M., 1995, A&A, 300, 441

Church M. J., Bałucińska-Church M., 2004, MNRAS, 348, 955

Church M. J., Gibiec A., Bałucińska-Church M., 2014, MNRAS, 438, 2784

Church M. J., Gibiec A., Bałucińska-Church M, Jackson N. K., 2012, A&A, 546, A35

Church M. J., Halai G. S., Bałucińska-Church M., 2006, A&A, 460, 233

Coburn W., Heindl W. A., Rothschild R. E., Gruber D. E., Kreykenbohm I., Wilms J., Kretschmar P., Staubert R., 2002, ApJ, 580, 394

Crary D. J., Finger M. H., Kouveliotou C., van der Hooft F., van der Klis M., Lewin W. H. G., van Paradijs J., 1988, ApJ, 493, L71

Cui W., 1999, ApJ, 524, L59

Ding G. Q., Zhang S. N., Li T. P., Qu J. L., 2006, ApJ, 645, 576

Ding G. Q., Zhang S. N., Wang N., Qu J. L., Yan, S. P., 2011, AJ, 142, 34

Di Salvo T., Robba N. R., Iaria R., Stella L., Burderi L., Israel G. L., 2001, ApJ, 554, 49

Focke W. B., 1996, ApJ, 470, L127

Ford E., Kaaret P., Tavani M., Barret D., Bloser P., Grindlay J., Harmon B. A., Paciesas W. S., Zhang S. N., 1997, ApJ, 475, L123

Ford E. C., van der Klis M., Méndez M., van Paradijs J., Kaaret P., 1999, ApJ, 512, L31

Hasinger G, van der Klis M., 1989, A&A, 225, 79

Homan J., van der Klis M., Fridriksson J. K., Remillard R. A., Wijnands R., Méndez M., Lin D., Altamirano D., Casella P., Belloni T. M., Lewin W. H. G., 2010, ApJ, 719, 201

Homan J., van der Klis M., Wijnands R., Belloni T., Fender R., Klein-Wolt M., Casella P., Méndez, M., Gallo E., Lewin W. H. G., Gehrels N., 2007, ApJ, 656, 420

Iaria R., D'Aí, di Salvo T., Robba N. R., Riggio A., Papitto A., Burderi L., 2009, A&A, 505, 1143

Ingram A., Done C., 2011, MNRAS, 415, 2323

Ingram A., van der Klis M., 2013, MNRAS, 434, 1476

Inogamov N. A., Sunyaev R. A., 1999, Astron. Lett., 25, 269

Inogamov N. A., Sunyaev R. A., 2010, Astron. Lett., 36, 848

Jackson N. K., Church M. J., Bałucińska-Church M., 2009, A&A, 494, 1059

Jahoda K., Markwardt C. B., Radeva Y., Rots A. H., Stark M. J., Swank J. H., Strohmayer T. E., Zhang W., 2006, ApJS, 163, 401

Lamb F. K., Pethick C. J., Pines, D., 1973, ApJ, 184, 271

Lee H. C., Misra R., Taam R. E., 2001, ApJ, 549, L229

Lei Y. J., Qu J. L., Song L. M., Zhang C. M., Zhang S., Zhang F., Wang J. M., Li Z. B., Zhang G. B., 2008, ApJ, 677, 461

Lei Y. J., Zhang H. T., Zhang C. M., Qu J. L., Yuan H. L., Dong Y. Q., Zhao Y. H., Wang D. H., Yin H. X., Zhang Y. X., Song L. M., 2013, AJ, 146, 60

Lei Y. J., Zhang S., Qu J. L., Yuan H. L., Wang Y. N., Dong Y. Q., Zhang H. T., Li Z. B., Zhang C. M., Zhao Y. H., 2014, AJ, 147, 67

Lin D., Remillard R. A., Homan J., 2009, ApJ, 696, 1257

Miller M. C., Lamb F. K., Psaltis D., 1998, ApJ, 508, 791

Mitsuda K., Inoue H., Koyama K., Makishima K., Matsuoka M., Ogawara Y., Suzuki K., Tanaka Y., Shibazaki N., Hirano T., 1984, PASJ, 36, 741

Mitsuda K., Inoue H., Nakamura N., Tanaka Y., 1989, PASJ, 41, 97

Miyamoto S., Kitamoto S., Iga S., Negoro H., Terada K., 1992, ApJ, 391, L21

Miyamoto S., Kitamoto S., Mitsuda K., Dotani T., 1988, Nature., 336, 450

Miyamoto S., Kitamoto S., 1989, Nature., 342, 773

Negoro H., Kitamoto S., Mineshige S., 2001, ApJ, 554, 528

Nobili L., Turolla R., Zampieri L., Belloni T., 2000, ApJ, 538, L137

Nowak M. A., 1994, ApJ, 422, 688

Nowak M. A., Vaughan B. A., Wilms J., Dove J. B., Begelman M. C., 1999a, ApJ, 510, 874

Nowak M. A., Wilms J., Dove J. B., 1999b, ApJ, 517, 355

O'Neill P. M., Kuulkers E., Sood R. K., van der Klis M., 2002, MNRAS, 336, 217

Oosterbroek T., van der Klis M., Kuulkers E., van Paradijs J., Lewin W. H. G., 1995, A&A, 297, 141

Pahari M., Neilsen J., Yadav J. S., Misra R., Uttley P., 2013, ApJ, 778, 136

Ponman T. J., Cooke B. A., Stella L., 1988, MNRAS, 231, 999

Poutanen J., Fabian A. C., 1999, MNRAS, 306, L31

Pottschmidt K., Wilms J., Nowak M. A., Heindl W. A., Smith D. M., Staubert, R., 2000, A&A, 357, L17

Poutanen J., 2001, in White N. E., Malaguti G., Palumbo G. G. C., eds, AIP Conf. Proc. Vol. 599, X-ray Astronomy: Stellar Endpoints, AGN, and the Diffuse X-ray Background. Am. Inst. Phys., Melville, NY, p. 310. arXiv:astro-ph/0002505

Qu J. L., Lu F. J., Lu Y., Song L. M., Zhang S., Ding G. Q., Wang J. M., 2010a, ApJ, 710, 836

Qu J. L., Lu Y., Ding G. Q., Zhang F., Lei Y. J., Li Z. B., 2010b, SCPMA, 53, 60

Qu J. L., Yu W., Li T. P., 2001, ApJ, 555, 7

Reig P., Belloni T., van der Klis M., Méndez M., Kylafis N. D., Ford E. C., 2000, ApJ, 541, 883

Revnivtsev M., Churazov E., Postnov K., Tsygankov S., 2009, A&A, 507, 1211

Shirey R. E., Bradt, H. V.. Levine, A. M., 1999, ApJ, 517, 472

Shakura N. I., Sunyaev R. A., 1973, A&A, 24, 337

Stella L., Vietri M., 1998, ApJ, 492, L59

Strohmayer T. E., Zhang W., Swank J. H., Smale A., Titarchuk L., Day C., Lee U., 1996, ApJ, 469, L9

Sriram K., Agrawal V. K., Pendharkar J. K., Rao A. R., 2007, ApJ, 661, 1055

Sriram K., Choi C. S., Rao A. R., 2012, ApJS, 200, 16

Sriram K., Rao A. R., & Choi C. S., 2010, ApJ, 725, 1317

Terrell N. J., Jr., 1972, ApJ, 174, L35

van der Hooft F., Kouveliotou C., van Paradijs J., Paciesas W. S., Lewin W. H. G., van der Klis M., Crary D. J., Finger M. H., Harmon B. A., Zhang S. N., 1999, ApJ, 513, 477

van der Klis M., 2000, ARA&A, 38, 717

van der Klis M., Hasinger G., Stella L., Langmeier A., van Paradijs J., Lewin W. H. G., 1987, ApJ, 319, L13

Uttley P., McHardy I. M., 2001, MNRAS, 323, L26

Vaughan B., van der Klis M., Lewin W. H. G., Wijers R. A. M. J., van Paradijs J., Dotani T., Mitsuda K., 1994, ApJ, 421, 738

Wang Y. N., Lei Y. J., Ding G. Q., Qu J. L., Ge M. Y., Zhang C. M., Chen L., Ma X., 2014, MNRAS, 440, 3726

Zhang W., Strohmayer T. E., Swank J. H., 1998, ApJ, 500, L167

Table 1. The results of cross-correlation analysis on the HID.

[a]HID Region	[b]Position	[c]Live Time (s)	[d]CCC	[e]Time Lag (s)	[f]Hardness
1	UNB	2023	0.68±0.05	4.0±1.2	0.78
2	UNB	3936	0.71±0.13	-1.0±3.0	0.76
3	UNB	4624	0.41±0.09	9.4±6.4	0.75
4	MNB	3752	0.72±0.13	2.0±2.6	0.73
5	MNB	3152	0.64±0.56	0.4±1.5	0.72
6	MNB	3648	0.68±0.08	0.7±2.1	0.70
9	LNB	6112	0.27±0.05	-36.4±9.2	0.65
10	LNB	2432	0.53±1.07	-6.1±7.5	0.64
11	LFB	8606	0.62±0.09	-0.1±2.4	0.65
12	LFB	4960	0.74±0.09	-2.6±1.9	0.66
13	LFB	3560	0.82±0.08	-0.2±1.5	0.67
14	LFB	4032	0.53±0.07	1.3±3.7	0.68
15	LFB	4080	0.95±1.24	-3.8±11.1	0.69
16	MFB	3360	0.88±0.88	-3.6±8.1	0.70
17	MFB	3168	1.63±6.45	7.1±3.3	0.71
18	MFB	2224	0.79±0.14	0.1±2.9	0.72
22	UFB	1072	1.49±5.88	-5.7±9.4	0.81
23	UFB	1232	0.87±0.11	0.8±2.2	0.83

[a]The regions in which positive correlations are detected.
[b]The positions of the regions.
[c]The total relative time length of each region.
[d]The derived cross−correlation coefficients.
[e]The derived time lags.
[f]The hardness.

Table 2. The results of anti-correlated correlations which are detected outside the period of the HID.

[a]ObsID	[b]Date	[c]CCC	[d]Time Lag (s)
30043-01-07-00	1998-10-09	-0.34±0.03	192±10
50017-01-02-00	2003-01-09	-0.21±0.01	1177±57
80105-05-01-00	2003-09-23	-0.72±0.02	-6107±46
90024-04-02-00	2004-04-17	-0.36±0.07	-77±5
90024-04-09-00	2004-08-02	-0.24±0.03	-327±16
90024-04-12-00	2004-09-22	-0.33±0.04	-66±10
90024-04-16-00	2005-01-08	-0.28±0.06	85±6
90024-04-21-00	2005-04-02	-0.24±0.05	258±20
93071-05-01-00	2008-09-17	-0.33±0.02	-127±15
93071-05-03-00	2008-09-26	-0.16±0.01	-25±27

[a]The observations in which anti-correlated correlations are detected.
[b]The observation dates.
[c]The derived cross−correlation coefficients.
[d]The derived time lags.

Table 3. The results of positive correlations which are detected outside the period of the HID.

[a]ObsID	[b]Date	[c]CCC	[d]Time Lag (s)
10063-11-01-00	1996-09-07	0.62±0.04	4.8±5.1
10063-12-01-00	1996-09-06	0.69±0.01	7.6±23.2
30043-01-01-00	1998-09-29	0.50±0.03	1.1±46
30043-01-02-00	1998-09-29	0.89±0.01	-2.5±2.9
30043-01-03-00	1998-09-30	0.35±0.03	39.3±9.6
30043-01-04-00	1998-09-30	0.85±0.03	24.1±7.7
30043-01-05-00	1998-10-01	0.78±0.02	-29.5±5.7
30043-01-06-00	1998-10-01	0.85±0.03	8.6±2.9
30043-01-08-00	1998-10-02	0.91±0.02	6.8±4.5
30043-01-09-00	1998-10-03	0.77±0.03	-18.7±5.9
30043-01-10-00	1998-10-03	0.54±0.03	6.3±7.8
30043-01-11-00	1998-10-04	0.65±0.03	-18.0±14.1
30043-01-12-00	1998-10-04	0.84±0.02	0.8±3.9
30043-01-13-00	1998-10-05	0.53±0.06	2.2±4.8
30043-01-14-00	1998-10-05	0.64±0.02	-18.1±6.0
30043-01-15-00	1998-10-06	0.63±0.04	64.4±14.0
30043-01-16-00	1996-09-07	0.94±0.05	-18.7±16.7
30043-01-17-00	1998-10-07	0.54±0.03	38.1±5.9
30043-01-18-00	1998-10-08	0.69±0.06	-18.1±14.4
30043-01-19-00	1998-10-08	0.80±0.03	-3.4±6.7
30043-01-20-00	1998-10-09	0.51±0.06	-4.0±7.7
30043-01-21-00	1998-10-09	0.82±0.03	-7.8±5.1
30043-01-22-00	1998-10-10	0.84±0.05	-29.3±16.0
30043-01-23-00	1998-10-10	0.83±0.07	-3.6±4.73
30043-01-24-00	1998-10-11	0.88±0.03	-13.0±9.7
30043-01-25-00	1998-10-11	0.33±0.05	7.7±12.0
30043-01-26-00	1998-10-12	0.54±0.04	5.1±17.0
30043-01-27-00	1998-10-12	0.70±0.05	-5.4±10.8
30043-01-28-00	1998-10-13	0.86±0.05	0.6±5.8
30043-01-29-00	1998-10-13	0.42±0.06	2.2±4.8
30043-01-30-00	1998-10-14	0.32±0.05	-30.7±10.3
50017-01-01-00	2000-03-27	0.20±0.04	42.5±20.2
50017-01-01-02	2000-03-29	0.85±0.05	-2.6±4.0
50017-01-01-03	2000-03-29	0.78±0.02	-20.6±8.1
50017-01-01-04	2000-03-29	0.74±0.02	3.7±7.9
50017-01-01-06	2000-03-29	0.68±0.05	-16.2±8.3
50017-01-01-08	2000-03-30	0.57±0.06	6.7±4.2
50017-01-01-09	2000-03-31	0.62±0.05	-3.1±12.4
90022-03-01-00	2004-08-05	0.82±0.05	1.5±8.9
90022-03-02-00	2004-08-21	0.77±0.03	-6.8±9.2
90022-03-03-00	2004-08-28	0.73±0.01	-13.6±5.9
90022-03-04-00	2004-09-04	0.77±0.07	10.2±4.6
90022-03-04-01	2004-09-05	0.86±0.02	47.7±19.9
90022-03-04-02	2004-09-07	0.25±0.02	-13.6±10.1
90022-03-04-03	2004-09-07	0.37±0.05	-29.3±11.9
90022-03-05-00	2004-09-15	0.85±0.05	-26.6±12.6
90022-03-05-01	2004-09-14	0.81±0.03	9.5±7.4
90022-03-07-00	2005-10-05	0.61±0.07	-13.3±10.8
90022-03-07-01	2005-10-06	0.84±0.05	-8.2±15.1
90022-03-08-00	2005-10-07	0.82±0.06	-0.2±6.2
90022-03-08-01	2005-10-07	0.69±0.02	1.4±6.2
90022-03-09-00	2006-10-12	0.32±0.03	30.4±14.2
90024-04-01-00	2004-04-02	0.75±0.05	-4.1±4.2

Table 3 – *continued*

[a]ObsID	[b]Date	[c]CCC	[d]Time Lag (s)
90024-04-02-01	2004-04-18	0.96±0.11	0.3±6.3
90024-04-02-02	2004-04-22	0.91±0.17	-1.9±8.4
90024-04-03-00	2004-05-21	0.54±0.04	20.8±16.0
90024-04-04-00	2004-05-28	0.80±0.07	-0.6±5.2
90024-04-06-00	2004-06-14	0.85±0.06	6.6±8.6
90024-04-07-00	2004-07-01	0.37±0.06	102.8±14.6
90024-04-08-00	2004-07-16	0.75±0.07	-0.1±3.2
90024-04-10-00	2004-08-13	0.84±0.10	-3.9±3.2
90024-04-11-00	2004-09-09	0.27±0.11	-13.8±8.4
90024-04-13-00	2004-10-12	0.74±0.05	5.2±11.1
90024-04-14-00	2004-10-26	0.71±0.05	-26.1±9.1
90024-04-15-00	2004-11-13	0.53±0.05	1.5±6.7
90024-04-17-00	2005-01-26	0.67±0.08	25.1±11.0
90024-04-18-00	2005-02-15	0.69±0.06	18.8±10.4
90024-04-18-01	2005-02-12	0.79±0.08	-0.9±1.6
90024-04-18-02	2005-02-16	0.87±0.06	-23.7±7.9
90024-04-19-00	2005-02-24	0.81±0.09	5.6±6.8
90024-04-20-00	2005-03-16	0.42±0.10	-22.1±9.7
90024-04-22-00	2005-05-17	0.82±0.09	-13.7±8.3
90024-04-23-00	2005-05-25	0.87±0.10	-4.0±3.2
90024-04-25-00	2005-06-17	0.80±0.05	-48.4±11.8
90024-04-26-00	2005-07-11	0.24±0.05	1.6±10.3
90024-04-27-00	2005-07-19	0.21±0.04	-4.0±6.1
90024-04-28-00	2005-08-11	0.90±0.09	0.2±1.6
90024-04-29-00	2005-08-25	0.38±0.03	-49.1±10.4
90024-04-31-00	2005-09-21	0.76±0.07	-5.1±2.3
90024-04-32-00	2005-10-10	0.60±0.08	-0.8±2.4
90024-04-33-00	2005-10-17	0.37±0.04	15.0±11.7
90024-04-34-00	2005-11-02	0.90±0.05	-42.7±9.9
90024-04-35-00	2005-11-11	0.88±0.06	6.7±3.3
90024-04-36-00	2006-01-16	0.53±0.04	-32.7±6.3
90024-04-37-00	2006-02-13	0.91±0.14	-7.2±8.8
90024-04-38-00	2006-02-18	0.80±0.09	2.8±1.8
90024-04-39-00	2006-03-10	0.61±0.03	28.1±9.1
90024-04-42-00	2006-05-05	0.70±0.06	6.3±6.7
90024-04-43-00	2006-05-21	0.89±0.05	0.3±0.9
90024-04-44-00	2006-06-18	0.73±0.07	-11.4±3.8
90024-04-45-00	2006-07-17	0.65±0.05	-13.7±11.4
90024-04-46-00	2006-08-05	0.83±0.05	2.6±3.3
91152-01-01-00	2006-05-10	0.70±0.01	6.3±8.5
91152-01-01-01	2006-05-10	0.87±0.03	3.7±6.4
91152-01-02-00	2006-07-04	0.85±0.02	135.7±27.4
91152-01-03-00	2006-08-20	0.62±0.02	16.0±18.9
93406-07-01-00	2007-07-05	0.81±0.03	50.0±13.5
96378-04-01-00	2011-07-06	0.46±0.01	-286.7±40.1
96378-04-01-01	2011-07-06	0.87±0.05	-1.4±9.4
96378-04-02-00	2011-10-09	0.74±0.01	-76.8±19.6

[a]The observations in which positive correlations are detected.
[b]The observation dates.
[c]The derived cross−correlation coefficients.
[d]The derived time lags.

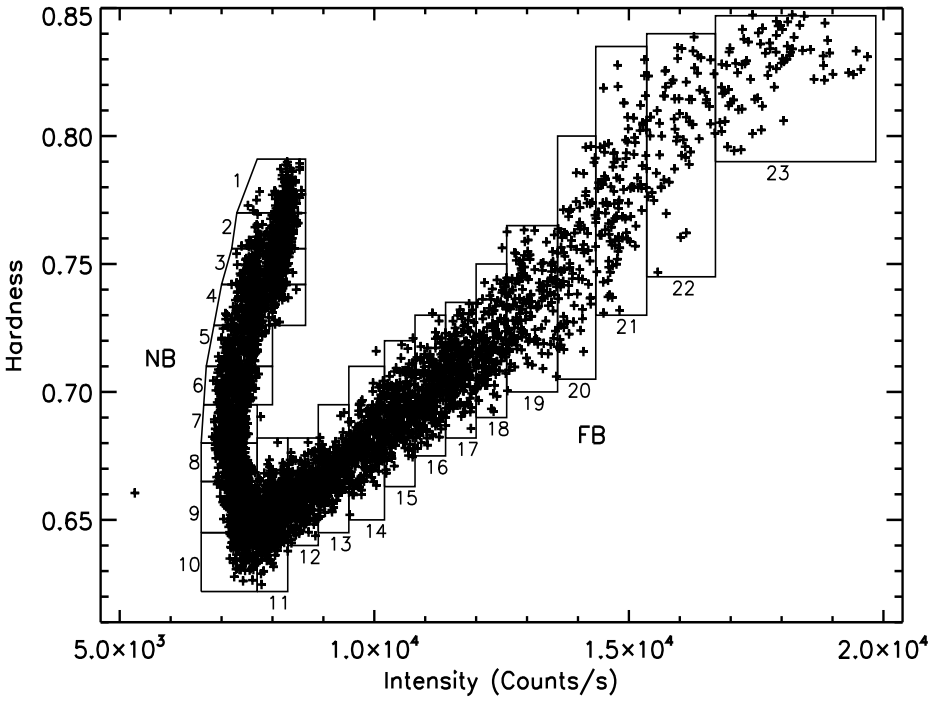

Figure 1. The HID of GX 349+2. Each point represents 16 s background-subtracted data. The hardness is defined as the count rate ratio between 8.7-19.7 keV and 6.2-8.7 keV energy bands, and the intensity as the count rate in the 2.0-19.7 keV energy band. In orde to investigate cross-correlation evolution on the HID, the track of the extensive Z track is divided into 23 regions (labeled 1, 2, ..., 23) that are used to group data for production of CCF of each region.

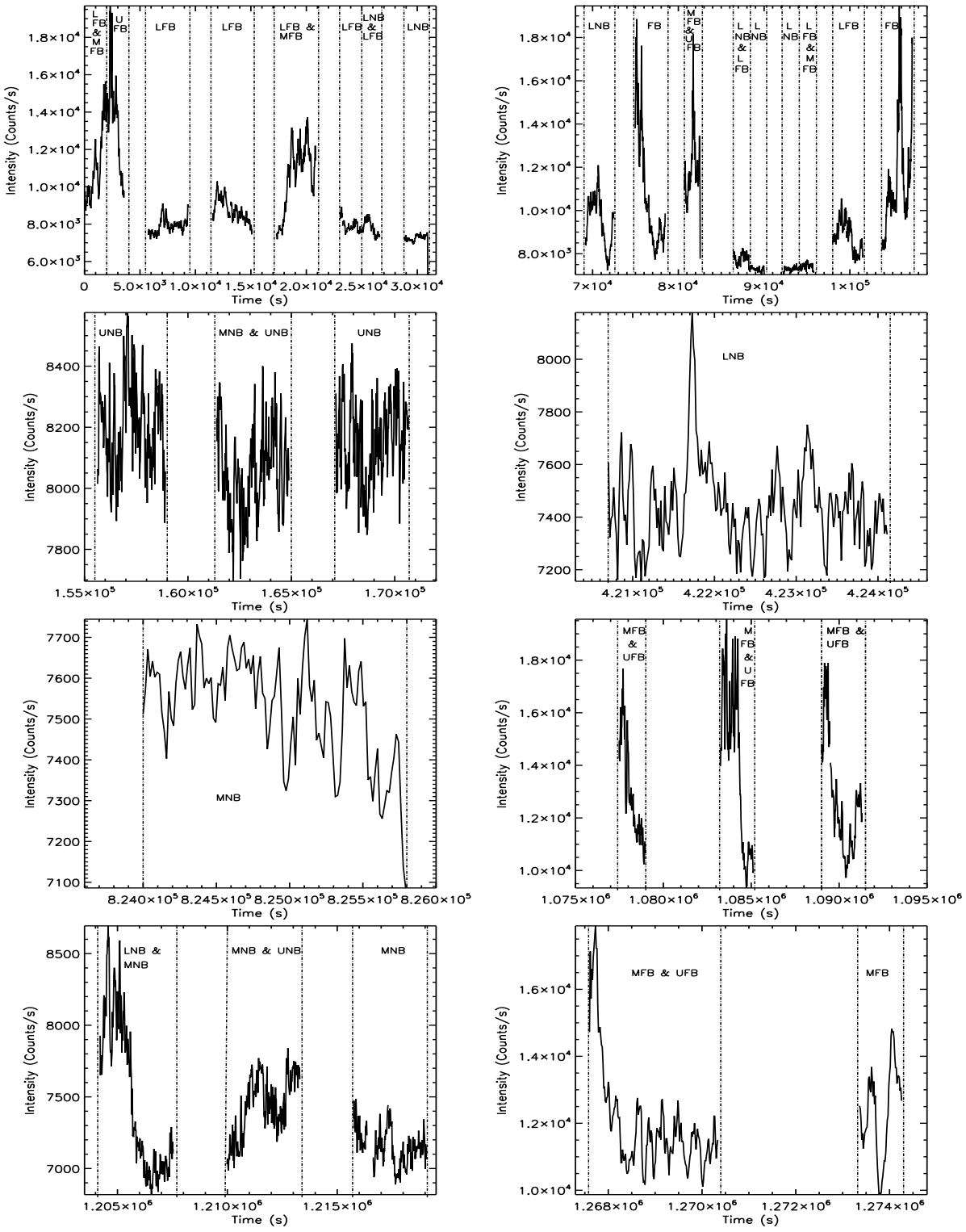

Figure 2. The light curve during the period tracing out the HID. The positions of segments on the HID are identified. The light curve shows that on the HID the source evolves from the FB to the NB and it shows two evolutionary cycles and the beginning of the third evolutionary cycle.

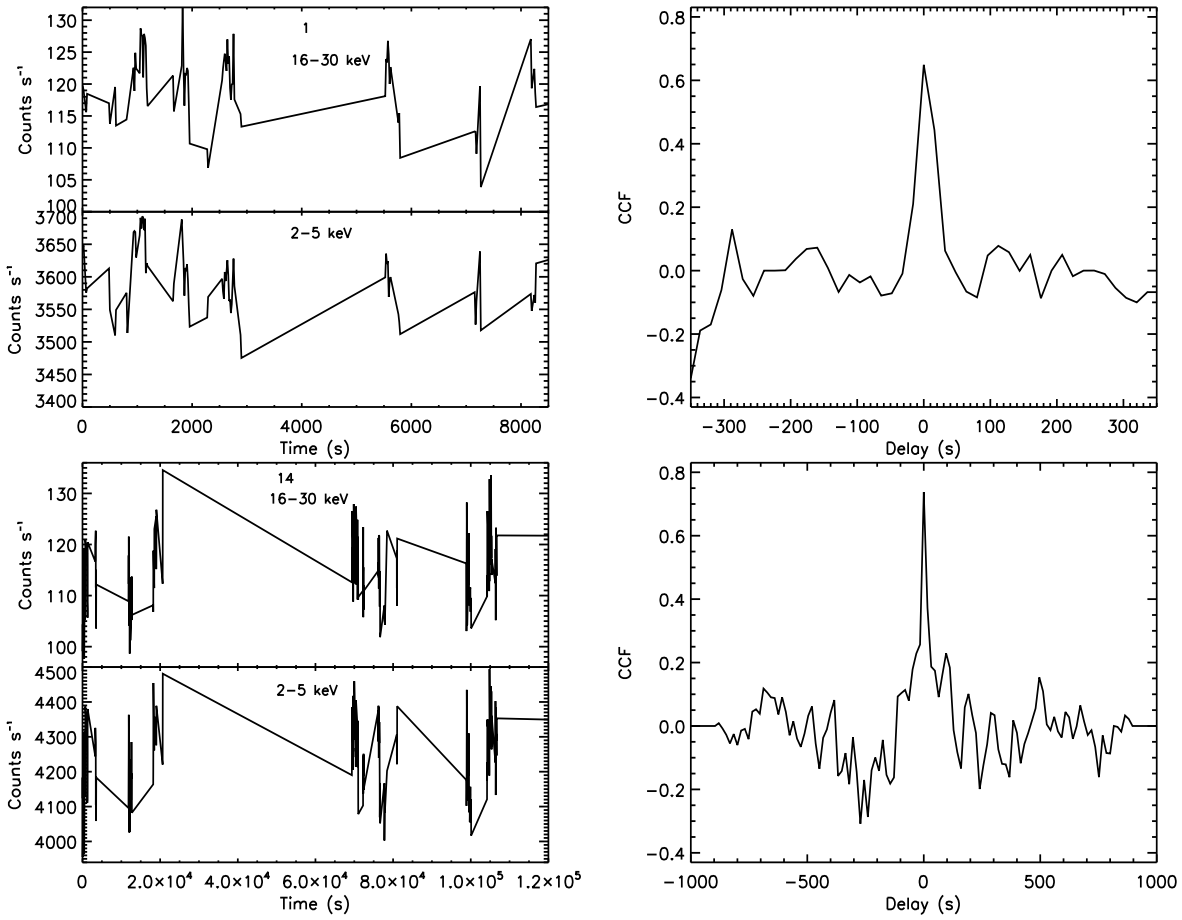

Figure 3. Left panels: the hard light curves (16-30 keV) and soft light curves (2-5 kev) of two representative HID regions (1, 14) in which positive correlations are detected. Right panels: the CCFs of the two regions.

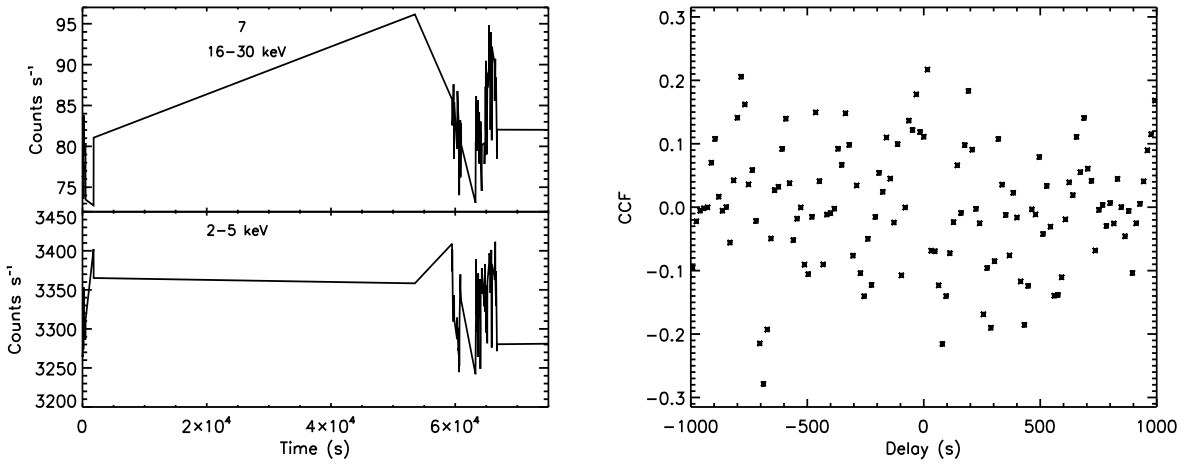

Figure 4. The upper and low panels on the left show the hard X-ray light curve (16-30 keV) and soft X-ray light curve (2-5 keV) of region 7 of the HID, respectively. The panel on the right shows the CCF of the two light curves, where a typical ambiguous correlation is shown.

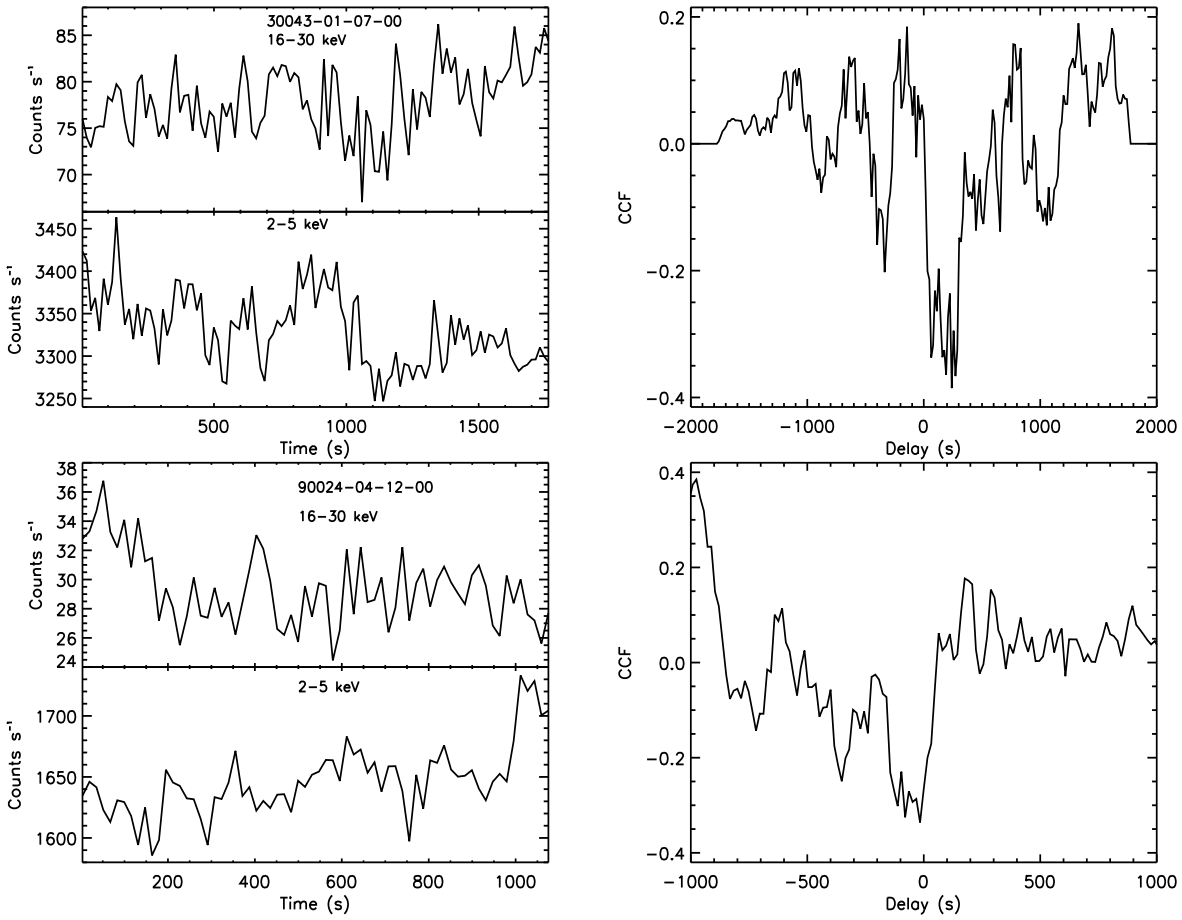

Figure 5. Two representative anti-correlated correlations which are detected in the epoch outside the period tracing out the HID. Left panels: the hard X-ray light curves (16-30 keV) and soft X-ray light curves (2-5 kev) of two observations in which anti-correlated correlations are detected; right panels: the CCFs of the two observations.